Lawrence Berkeley National Laboratory
LBL Publications

Title
High-density electrical and optical probes for neural readout and light focusing in deep brain tissue

Permalink
https://escholarship.org/uc/item/0r43g2x8

Journal
Journal of Micro/Nanopatterning Materials and Metrology, 17(2)

ISSN
1932-5150

Authors
Lanzio, Vittorino
West, Melanie
Koshelev, Alexander
et al.

Publication Date
2018-04-01

DOI
10.1117/1.jmm.17.2.025503

Peer reviewed

High-density electrical and optical probes for neural readout and light focusing in deep brain tissue

Vittorino Lanzio
Melanie West
Alexander Koshelev
Gregory Telian
Paolo Micheletti
Raquel Lambert
Scott Dhuey
Hillel Adesnik
Simone Sassolini
Stefano Cabrini

High-density electrical and optical probes for neural readout and light focusing in deep brain tissue

Vittorino Lanzio,[a] Melanie West,[a,b] Alexander Koshelev,[c] Gregory Telian,[b] Paolo Micheletti,[a] Raquel Lambert,[a] Scott Dhuey,[a] Hillel Adesnik,[b] Simone Sassolini,[a] and Stefano Cabrini[a,*]
[a]Lawrence Berkeley National Laboratory, Molecular Foundry, Nanofabrication Facility, Berkeley, California, United States
[b]Berkeley University of California, Adesnik Lab, Berkeley, California, United States
[c]aBeam Technologies, Hayward, California, United States

Abstract. To advance neuroscience *in vivo* experiments, it is necessary to probe a high density of neurons in neural networks with single-cell resolution and be able to simultaneously use different techniques, such as electrophysiological recordings and optogenetic intervention, while minimizing brain tissue damage. We first fabricate electrical neural probes with a high density of electrodes and small tip profile (cross section of shank: 47-μm width $\times$ 16-μm thickness). Then, with similar substrate and fabrication techniques, we separately fabricate optical neural probes. We finally indicate a fabrication method that may allow integrating the two functionalities into the same device. High-density electrical probes have been fabricated with 64 pads. Interconnections to deliver the signal are 120-nm wide, and the pads are 5×25 μm. Separate optical probes with similar shank dimensions with silicon dioxide and silicon nitride ridge single-mode waveguides have also been fabricated. The waveguide core cross section is 250 nm $\times$ 160 nm. Light is focused above the waveguide plane in 2.35-μm diameter spots. The actual probes present two output focusing gratings on the shank. © *The Authors.* Published by SPIE under a Creative Commons Attribution 3.0 Unported License. Distribution or reproduction of this work in whole or in part requires full attribution of the original publication, including its DOI. [DOI: 10.1117/1.JMM.17.2.025503]

Keywords: neural probes; high density; light focusing; integration.

Paper 18007 received Jan. 11, 2018; accepted for publication Jun. 4, 2018; published online Jun. 30, 2018.

1 Introduction

One of the main goals of the Brain Research through Advancing Innovative Neurotechnologies (BRAIN) Initiative [1] is to map the brain at the single neuron and synapse level to understand how neural communication drives behavior and affects brain disorders. Nanotechnology has opened new pathways to interface single brain cells *in vivo* in brain tissue due to dimensions comparable to neural cells and the feasibility of integration of different types of sensors. In particular, Michigan neural probes are invasive devices built on a silicon (or polymeric) substrate.[2] Michigan neural probes allow the use of micro and nanofabrication techniques (which imply high yield, low defectivity, and scalability) and integrate a high density of arrays of sensors (density limited mainly by the lithography resolution). The main element of these type of brain–machine interfaces is a sharp silicon tip (the shank) that is inserted into the animal's brain and which contains passive or active sensors [electrodes,[3,4] microfluidic channels,[5] optical diffraction gratings,[6] and micro-light-emitting diodes (LEDs)[7]]. Sensors on the shank are connected, due to metallic interconnections, waveguides, or microfluidic channels, to an extracranial device region having bond pads,[8] optical coupling gratings, or fluidic interfaces.[5] Many *in vivo* neuroscience studies employ Michigan neural probes to record or stimulate neurons by means of different types of techniques. Among these, invasive electrophysiology measurements (performed due to

electrodes on the device's shank) provide information on cortical circuit communication around the device through the recording of extracellular potentials.[9] Another technique, optogenetics, uses light to manipulate neural population activity. Specific types of neurons are genetically modified by the introduction of opsins in the brain using viral vectors or anatomical targeting strategies.[10,11] Channelrhodopsins are light-sensitive proteins that are able to enhance or inhibit neural population activity in the presence of light with the correct wavelength (around 450 to 473 nm).[12] Different studies involving the manipulation of neural populations using optogenetic tools have shown promising future applications in brain disorders research.[13,14] The simultaneous use of both electrophysiology and optogenetics in the same experiment is a necessary step to evolve neuroscience experiments.[15,16] Different methods allow achieving multipoint and patterned illumination, for example, with tapered fibers[17] or patterned photostimulation.[18,19] These methods do not allow the coupling of electrophysiology devices in close proximity and are not scalable. Michigan neural probes have shown the feasibility of integrating both types of sensors and of scaling the device size.[2] In fact, the shank of such devices can be miniaturized (tip widths larger than 60 μm decrease the quality of recordings)[20] while the sensor density can be increased (to interface simultaneously larger number of neurons).[21] Current electro-optical *in vivo* experiments rely on illuminating a broad neural population by integrating micro-LEDs next to electrodes[22] or by coupling the probe with waveguides.[8] All these methods present issues, such as heat generation[23] (for micro-LEDs), and the resulting shanks cannot be scaled (due to the large size of the

*Address all correspondence to: Stefano Cabrini, E-mail: Scabrini@lbl.gov

shown micro-LEDs and waveguides). Interesting and scalable photonic probes with silicon nitride waveguides have been proposed in Refs. 6 and 24 but only the photonic part has been shown. In this paper, we propose a fabrication method to integrate arbitrarily designed optical and electronic circuits on a single device. In this regard, we fabricate probes with electronic circuits. Separately, we fabricate photonic probes with similar substrate and fabrication techniques used for fabricating the electronic probe. To interface complex neural networks with a high density of sensors and minimized tissue damage, we first developed Michigan neural probes with minimal shank dimensions (47-μm width and 16-μm thickness) and, to the best of our knowledge, the highest presented density of electrodes and interconnections for a single-layer probe (64 electrodes, 120-nm wide interconnecting wire). To gain precise control of few neural cells during *in vivo* experiments, a micrometric spatial confinement of light is necessary. Our optical probes can focus light above the device plane, due to the use of a focusing grating. The result consists of a light cone, which allows having the maximum of light intensity far from the shank, where neuron density is reduced due to device insertion.[25] Finally, we show that both electrical and optical probe versions have similar substrate and most of the fabrication processes. These fabrication techniques show the viability of fabricating a neural probe that is multifunctional, with minimal shank dimensions and high density of sensors, and can focus light deep in brain tissue.

2 Material and Methods

2.1 Fabrication

#### 2.1.1 Neural probes with electrodes: design and fabrication

Neural probes with a high density of electrodes are shown in Fig. 1. The effective shank is 900-μm long, 47-μm wide, and 16-μm thick [Fig. 1(a)]. Each shank hosts 64 electrodes with interconnections on a single layer. To accommodate such a high density of connections without using multilayer

processes, electron-beam lithography, metal evaporation, and lift-off techniques are utilized. Wires are as small as 120 nm in width and 450 nm in pitch [Fig. 1(b)]. Wires can also be further scaled down to 65 nm in width and 240 nm in pitch [128 electrodes can fit inside a 45-μm-wide shank with a single interconnection layer, see Fig. 1(c)]. Electrodes are 5-μm wide and 25-μm long, with a spacing of 2.5 μm. The fabrication process (Fig. 2) uses silicon substrates with a double-sided polished Si substrate with 100-nm Si_3N_4 layer, as a KOH etch mask [Fig. 2(a)]. On the wafer's frontside, a positive photoresist, ZEP 520 A, is spun at 4000 rpm. and exposed at 100 kV with a Vistec VB300 electron-beam lithography system. After exposure, the resist is developed in amyl acetate for 1 min, using ultrasonication to improve resist contrast [Fig. 2(b)]. Electrical circuits are, therefore, defined by evaporation of 10 nm of titanium and 100 nm of gold [Fig. 2(c)] and then by a lift-off process (PG remover 1 h, 80°C) [Fig. 2(d)]. No sonication is utilized during the lift-off process to reduce the interconnection defectivity. A thin SiO_2 layer (75 nm) passivates the interconnecting wires [Fig. 2(e)]. We deposit such a layer with an atomic layer deposition (ALD) tool (Oxford FlexAl, Plasma-Enhanced ALD, at 40°C). The ALD allows obtaining very high conformal, low stress, and thin passivation layers. To open the passivation layer on the electrodes, another electron-beam exposure (same parameters as the previous one) and a dry etching process are performed. This last step is done using a reactive ion etcher (RIE) tool (Oxford Plasmalab 80, using 35-sccm CHF_3 and 25-sccm Ar, with RF = 100 W and 30 mTorr of pressure). Thin membranes (15- to 25-μm thick) are defined on the wafer's backside [Fig. 2(f)] using the following processes. First, a UV photolithographic step (positive photoresist, MA-P 1215) defines the mask for the backside silicon nitride etching. Then, the backside nitride is etched (RIE, CHF_3, and O_2 with RF = 100 W and 55 mTorr of pressure). The wafer front is afterward protected with ProTek B3.[20] ProTek B3 allows protecting the metal lines on the wafer's frontside during the subsequent backside silicon etching. The thin membranes are finally
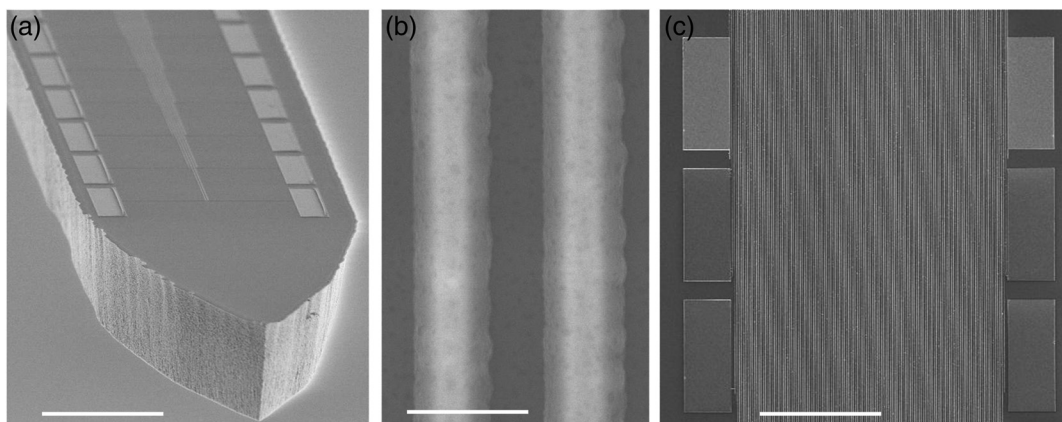
Fig. 1 Neural probes with high-density array of electrodes. (a) SEM image showing a zoom on device shank (thickness: 16 μm and width: 47 μm) and the 64 electrodes. Scale bar: 20 μm. (b) Zoom on interconnections (120-nm wide and with 450-nm pitch), passivated with 75 nm of SiO_2 (darker edge around interconnections). Scale bar: 200 nm. (c) View of wires (65-nm wide and 240-nm pitch). A total of 128 electrodes are defined on a single layer. Scale bar: 10 μm.
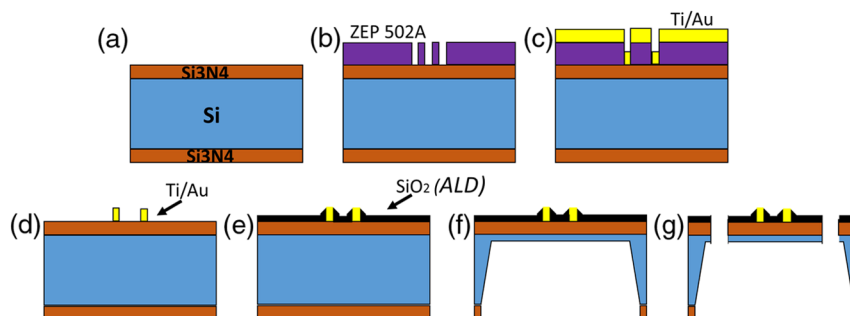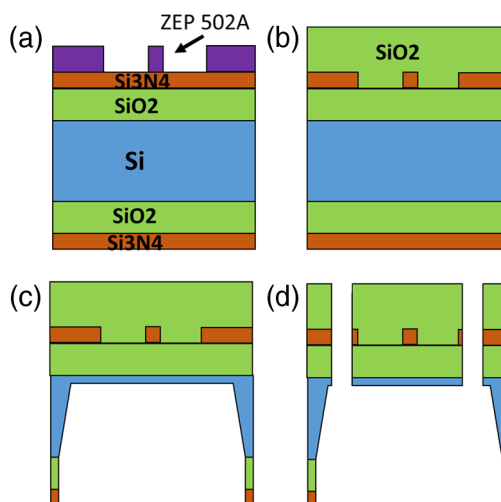
Fig. 2 Fabrication process of neural probes with high density of electrodes. (a) Starting wafer, (b) electron-beam exposure to define electrodes and interconnections, (c) titanium and gold evaporation, (d) lift-off in hot solvent, (e) deposition and etch after electron-beam lithography to open the passivation layer (75-nm SiO$_2$, ALD), and (f) backside etch to thin the probes. The silicon is etched in 33% KOH. (g) The probe shape is then defined by front side dry etch.

obtained by wet etching the silicon (33% KOH at 80°C, for 6 h) on the wafer's backside wherever the nitride mask had been previously removed. Once thin membranes are obtained, the ProTek layer on the front side is removed (2 h in Protek Remover 110).[26] Probes are defined onto the thin membranes by dry etching techniques onto the wafer's frontside [Fig. 2(g)]. A 180-nm chromium mask is deposited by electron-beam evaporation, and then a photo-lithographic step defines the probe shape with a 100-μm-wide trench. The pattern is transferred to the chromium (wet etching in chromium etchant 1020, 4 min) and Si$_3$N$_4$ layers (dry etching with RIE) and finally in the silicon with an inductively coupled plasma (ICP) RIE (Oxford PlasmaLab 150 ICP, using 44-sccm SF$_6$ and 6 sccm of O$_2$ at −120°C) to make free-standing probes. This last step is performed at cryogenic temperature to achieve straight sidewalls.[27] Free-standing probes are then soaked in chromium etchant 1020 to remove the residual chromium layer.

2.1.2 Neural probes with optical components: design and fabrication

Si$_3$N$_4$ − SiO$_2$ waveguide elements can propagate waves in the visible wavelength range, where opsin activation takes place, with low absorption losses. Neural optical probes are designed with a main input single-mode waveguide, with core cross section of 250 nm × 160 nm, and two focusing gratings (one at half-length of the shank and the other near the tip). Focusing gratings are diffractive optical elements that can extract the light from a waveguide and focus it perpendicularly above the plane. Neural probes with optical elements are fabricated using a similar substrate and fabrication process as the probes with electrodes. Lionix TriPleX wafers[28] are made of a stack of silicon (525 μm), double-side SiO$_2$ [2.5 μm, low pressure chemical vapor deposition (LPCVD) by Lionix] and Si$_3$N$_4$ (160 nm, LPCVD, by Lionix). Such wafers have been chosen since they present low absorption losses. An electron-beam lithography step (ZEP 520 A) defines the mask for waveguides and diffraction gratings [Fig. 3(a)]. The development is performed at room temperature in amyl acetate without sonication. The pattern is then transferred to the silicon nitride [Fig. 3(b)] (RIE, 48 sccm of CHF$_3$ and 2 sccm of O$_2$, with a pressure of 55 mTorr and an RF of 50 W) and covered with a 1.9-μm SiO$_2$ cladding layer [plasma enhanced chemical vapor deposition (PECVD) at 150°C, using 850-sccm 1% SiH$_4$/Ar and

710-sccm N$_2$O]. Probes are thinned by backside etching [Fig. 3(c)] to form thin membranes (55-μm thick). First, the nitride and oxide backside layers are removed through dry etching. A chromium layer (180 nm) is evaporated on the wafer's backside and is used as a mask for the dry etching of the nitride and oxide layers on the wafer's backside. The chromium mask is defined by optical photolithography (MA-P 1215) and wet chromium etching. The silicon nitride is etched in an RIE tool (same as the electrical version), and the SiO$_2$ layer is etched at −100°C in an Oxford Plasma lab 100 Viper (using a mix of 180-sccm SF$_6$ and 20-sccm Ar, with 400 very high frequency and 250 RF). The silicon is then thinned in a 33% KOH bath (at 85°C) (the wafer's front-side is protected, during the silicon etching, by ProTEK) and the ProTEK is finally removed. The probe shapes are defined from the wafer's frontside [Fig. 3(d)] by etching the SiO$_2$ (ICP, SF$_6$ and O$_2$ at −100°C), then the Si$_3$N$_4$ (RIE, using CHF$_3$ and O$_2$), again the SiO$_2$ (ICP, SF$_6$ and O$_2$ at −100°C), and the remaining silicon (ICP, SF$_6$ and O$_2$ at −120°C). The process uses a chromium mask (250 nm) patterned with optical photolithography and etched in chromium etchant 1020.

Fig. 3 Fabrication process of neural probes with optical elements. (a) Electron-beam exposure to define waveguides and gratings, (b) Si$_3$N$_4$ etching and cladding deposition (SiO$_2$, PECVD), (c) wafer's backside etch in 33% KOH, and (d) dry etch to define probes on the front side.

The remaining chromium is removed by soaking the obtained free-standing probes in chromium wet etchant.

2.1.3 *Electrical neural probe and optical neural probe assembly*

Electrical neural probes must be interfaced with external electronics—signal recording, amplifiers, and frequency filters—to read neuron electrical exchanges. A custom-made printed circuit board (PCB) is designed for this purpose. Our PCB is 6-mm wide near the shank and 60-mm long. On one side, we have pads for wire bonding; while on the other side, there are pads for Samtec 40-pins connectors. Probes are manually glued to the PCB and are wire bonded. Optical neural probes require an input light source. For this purpose, an optical fiber is used to couple with the laser source. The fiber that has a core diameter of 4 μm and 125-μm-diameter cladding is aligned to the waveguide and glued to the PCB. The fiber is initially aligned using a holder with a V-groove. The holder itself is mounted on a linear stage with microstepper motors. The alignment has submicrometric accuracy and minimal drift over time (fiber—waveguide coupling is maintained during the alignment and gluing of the fiber). On the other end, the fiber is connected to a fiber splitter with a blue (405 nm) and a green (520 nm) laser. UV curable glue (NOA 86, from Norland Products) is dispensed between the fiber tip and the waveguide edge. The alignment is performed using the 520-nm laser and adjusting the holder position. Once the alignment is done (a camera records the intensity of a probe output spot), the 405-nm laser is turned on to cure the glue. Extra glue is dispensed between the fiber holder and the PCB to render the system more stable and is cured with a UV gun. Once glued, the fiber cannot shift anymore.

2.1.4 *Electro-optical neural device integration*

As stated above, the final goal is to be able to read out and manipulate single neurons activity in complex networks using simultaneously electrical and optical sensors. With respect to this, it is worth noting that (1) both electrical probes and optical probes use similar substrates (waveguides and electrodes are fabricated on silicon nitride) and (2) most of the fabrication steps are the same for both versions. An electro-optical probe will, therefore, have both layers, with waveguides buried below the electrodes [Figs. 4(a)–4(c)]. In particular, we want to have waveguides and electrodes separated by a 2.5-μm-thick SiO$_2$ layer to keep light from scattering due to the gold interconnections. Electrodes and wires can cover all the optical features except for the focusing gratings. This method may allow achieving a simultaneous high density of electrode sites in combination with arbitrarily designed optical circuits. Optical circuits can be designed such that brain illumination is localized in the areas of interest. Light localization is obtained due to the gratings, which can be realized in multiple points along the shank. As an example, in Fig. 4(d), we show a design of optoelectronic probe with four buried optical waveguides each one having multiple gratings. A cross-section schematic is shown in Fig. 4(e)

3 Results

3.1 *Neural Probe Electrodes: Impedance Measurements and In Vivo Test*

The neural probe is glued on the PCB and wire bonded [Fig. 5(a)]. Impedance is measured in saline with a NanoZ commercial system (Neuralynx) and shows an average of 4.5 ± 0.1 MΩ at 1000 Hz before electroplating. Electroplating in a black platinum solution (Neuralynx) is
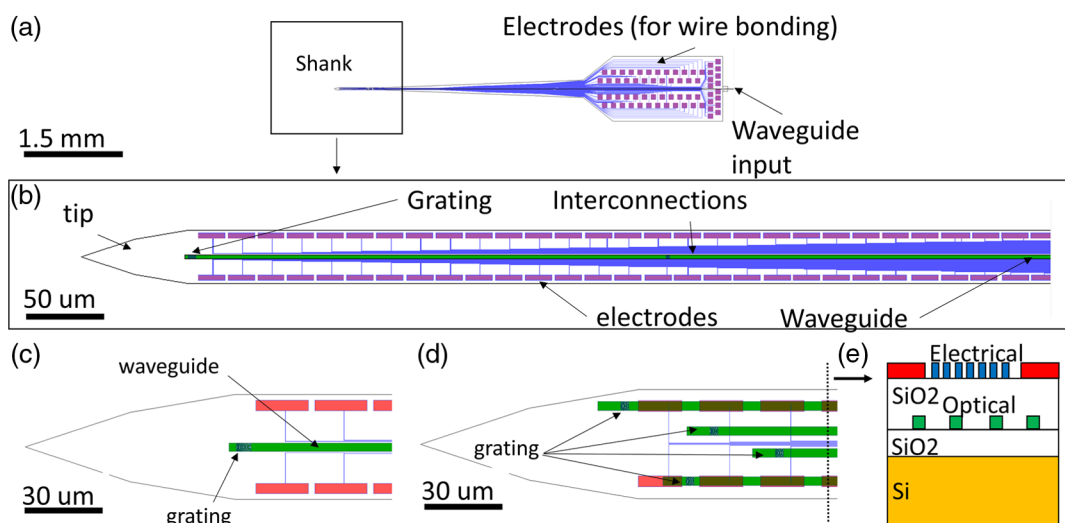
Fig. 4 Schematic of the integrated optoelectronic probe. (a) Probe top view: the larger part has electrodes for wire bonding to the PCB and the waveguide input. The thinner part is the shank, which is inserted in the mice brain. (b) Zoom on the shank, showing electronic circuits (red: electrodes and blue: interconnections) and photonic circuits (in green). (c) Zoom near the tip, showing the grating. (a), (b), and (c) designs correspond, separately, to the fabricated electrical and optical probes. (d) Design example of a more complex photonic circuit with a high density of light output spots. Four waveguides are shown (although more could fit in the shank). Waveguides could be connected, for example, by splitters. (e) Cross section of (d). Electronic and photonic circuits are independent and can, therefore, occupy the entire shank area.
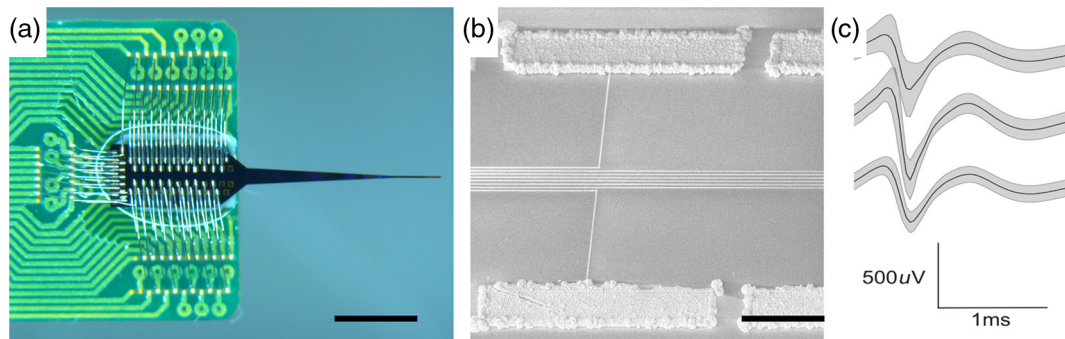
Fig. 5 (a) The probe is glued on the PCB and wire bonded. Scale bar: 2 mm. (b) SEM image, showing electroplated pads on the shank. Scale bar: 10 μm. (c) Plot of the mean (black) and standard deviation (gray) single-neuron waveforms recorded from three adjacent electrodes on the neural probe. For each of the three contacts, we plotted the largest amplitude of single-neuron signal recorded.

also achieved using the NanoZ by applying a DC current of -0.1 μA for 12 s [Fig. 5(b)]. Electroplating lowers the average electrode impedance down to 200 ± 30 KΩ at 1000 Hz. *In vivo* experiments were conducted using head-fixed mice in the Adesnik Lab, UC Berkeley. Mice used for experiments were either wild type (ICR white strain from Charles River Laboratories) or Ai32-PV-Cre mice that express the excitatory opsin channelrhodopsin (ChR2). All experiments were performed in accordance with the guidelines and regulations of the Animal Care and Use Committee of the University of California, Berkeley (Protocol # AUP-2014-10-6832). A small craniotomy was made right above whisker somatosensory cortex (aka barrel cortex). This is where inputs from the whiskers cause neurons to spike vigorously to sensory contacts. The small probe shank was rigid enough to pierce the dura matter. While the mouse was running, a bar was placed in the sector swept out by the whiskers, which typically generates robust sensory activity in barrel cortex. After probe insertion and recording, spike sorting was conducted using the automated spike sorter Klusta. This spike sorter used probe geometry and an advanced algorithm to detect single units. After the automated step, we use the provided graphical user interface to manually curate the data. Spikes that have reasonably shaped waveforms, low refractory period violations, good separation in PCA space, and good autocorrelograms are accepted as coming from a single unit.[29] Main single-neuron waveforms for three adjacent electrodes are shown in Fig. 5(c).

3.2 Optical Neural Probe Light Focusing, Fiber Alignment, and Output Power

Neural probes with an input waveguide and two focusing gratings on the shank are fabricated, assembled, and characterized. One focusing grating is placed at half shank length and the other at 60 μm from the tip. Figure 6(a) shows a zoom on the last part of the shank, where one of the two output spots is (laser input in the waveguide: 520 nm). The waveguide input has a core cross section of 250 nm (width) and 160 nm (height). This ensures that only the fundamental mode propagates (waveguides are, therefore, single mode). At 500 μm from the input, the waveguide is tapered to a width of 4 μm. Large waveguide width of 4 μm reduces sidewall scattering losses. The taper is 150-μm long and allows for adiabatic mode conversion between narrow and wide waveguide sections. Single-mode regime is necessary

to avoid multimode interference in the focusing gratings. Focusing gratings are diffractive optical elements that reconstruct the focus in a spot above the light propagation plane. These diffractive elements act like an integrated optical diffraction lens: light propagating in the waveguide is diffracted by chirped and curved grooves that deflect light rays at different angles; the light ray intersection point is the focal point.[30] The beam shape consists, therefore, of a light cone. The maximum of intensity of the beam is far from the shank plane (at the focusing height, which depends on the initial design of the grating), where neural cell density is reduced due to tissue damage during device insertion (the kill zone).[31] Such illumination may activate, in the light cone, one or more neurons. The focusing height and beam angle depend on the initial design of the grating. Gratings are scripted in MATLAB according to the formula presented in Ref. 32. Different wavelengths can be extracted for a fixed grating design. As shown in Ref. 30, a different wavelength will result in a different diffraction angle and beam focusing height. Different wavelengths can be, therefore, employed to activate different optogenetic actuators.[33] As an example, we couple, in the same probe shown in Fig. 6(a), other wavelengths [Figs. 6(b) and 6(c): 520 nm + 650 nm; Figs. 6(d) and 6(e): 450 nm + 650 nm]. Different types of beam shape can be obtained by choosing a different design for the grating. For example, a grating with parallel lines would collimate the output beam (with small divergence angle). Different types of gratings can be designed based on the *in vivo* experiments results. Future *in vivo* tests will allow engineering the optimal spot size, focal height, and optimal input power to trigger action potentials.

Waveguide losses are measured using test structures to be 8.1 dB/cm for blue light (450 nm) and 5.4 dB/cm for red light (650 nm). We designed two types of focusing gratings, one for red light (650 nm, focusing height: 10 μm) and one for blue light (450 nm, focusing height: 20 μm). Focusing grating output spots are imaged by a CCD camera and measured at different heights with respect to the grating plane. Measurements are performed in air. For the 650-nm grating, at the height of 10 μm (the grating focusing distance), the spot intensity is maximum and its full width at half maximum (FWHM) is measured to be 1.65 μm (data not shown). For the 450-nm grating, at the focusing height of 20 μm, the FWHM is 2.35 μm [Fig. 7(a)]. The grating lens is shown in Fig. 7(b). Images of spots at different CCD heights can be seen in Fig. 7(c). The majority of losses,
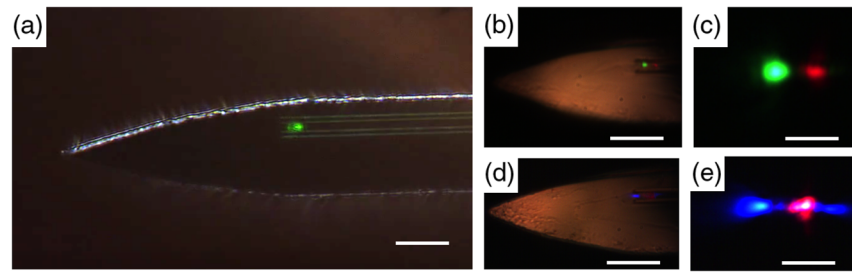
Fig. 6 (a) Neural probe with a waveguide and two focusing gratings. The image shows the grating near the tip. Light input: 520 nm. Scale bar: 15 μm. (b) Zoom on the tip. Laser input: 520 nm + 650 nm. Scale bar: 30 μm. (c) Zoom on the focusing grating output spots. Scale bar: 4 μm. (d) Probe tip with laser input 450 nm + 650 nm. Scale bar: 30 μm. (e) Zoom on the focusing grating output spots. Scale bar: 4 μm.
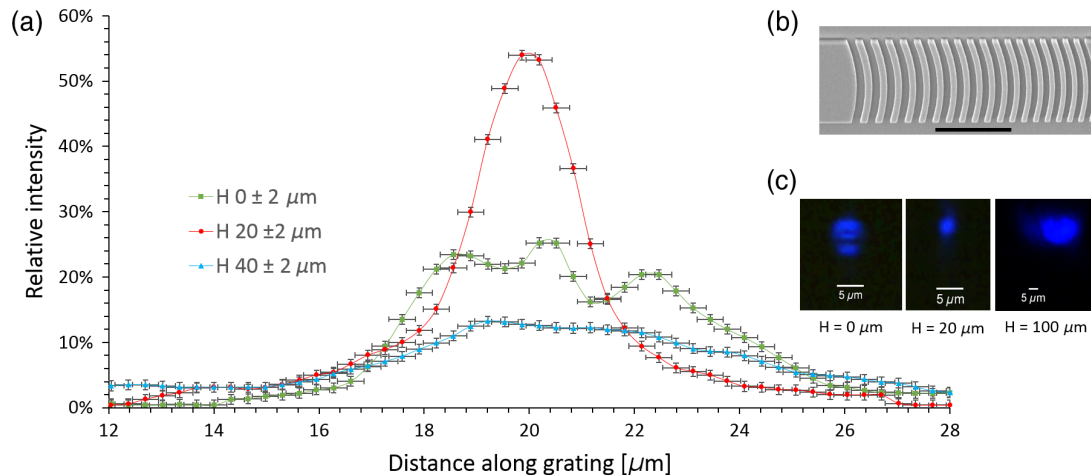
Fig. 7 (a) Relative intensity of the output spot of the probe focusing grating. The grating shown is been designed for blue light (450 nm), with a focusing height of 20 μm above the device plane. The intensity is plotted as function of a line along the focusing grating direction. The three curves show the image intensity recorded at different heights with respect to the grating's plane ($h = 0$ means the camera focus lies on the grating and $h = 10$ means the camera focus is 10 μm above the grating plane); error bars for the vertical axis correspond to noise (in plane scattered light). Error bars on the horizontal axis correspond to the pixel size. (b) SEM image of the probe focusing grating. (c) Output spot images at different camera heights. Left: CCD camera focused on grating plane. Center: CCD camera focused 20 μm above the grating plane (the focal plane). Right: CCD camera focused 100 μm above the grating plane; after the focusing point, the beam broadens.

estimated to be around 33 dB, are at the probe base (so far from the shank), where the fiber is aligned to the input waveguide on the probe. These high losses are due to a non-optimal fiber to waveguide coupling (fiber misalignment during glue curing). Focusing grating output coupling efficiency is estimated to be between 3.5 and 6 dB. The efficiency varies with the wavelength due to interferences between light extracted upward by the grating and light extracted downward and reflected at the bottom oxide cladding–silicon interface. To activate channelrhodopsins, a threshold of 1.5 mW/mm^2[34] is required. This translates to a power density of 1.5 nW/μm^2. The spot intensity on the neural probe is calculated after aligning the fiber and gluing it. Once glued, the fiber does not move, and therefore, the probe output power does not change for a fixed laser input power. The intensity value in the focusing point, with a laser input of 2 mW, equals 35.5 nW at half shank and 8.75 nW for the grating near the tip. This corresponds, at the focusing height (spot area: 5.5 mm^2), to a power density of 6.43 mW/mm^2 for the grating at half shank and 1.58 mW/mm^2 for the grating near the tip. These results

highlight the possibility of achieving neuron light activation that occurs within close proximity to the focused spot. The volume pertaining to the light cone, where channelrhodopsins can be activated, can be enlarged by increasing the laser power.

4 Conclusions

A deeper understanding of mechanisms underlying brain function and brain disorders requires neural network electrical readout and optical manipulation at the single-cell level. To answer these demands, we first fabricate a device with shank dimensions as small as 47 μm (width) × 16 μm (thickness), which is able to perform electrical readout of neural activity. We then separately fabricate optical neural probes to perform optogenetic excitation at different visible light wavelengths (*in vivo* results not presented in the paper). The example of photonic devices presented here has two light extraction points. More complex photonic circuits could be designed to increase the stimulation point density. Both electrical and optical devices are fabricated using similar substrate and fabrication techniques. This method

should, therefore, allow integrating both optical and electrical functionalities into a single device. We expect these results to help move brain science toward a more precise manipulation of light inside deep brain tissue for cell optical manipulation in *in vivo* neuroscience experiments in combination with electrical readouts.

References

1. L. A. Jorgenson et al., "The BRAIN Initiative: developing technology to catalyse neuroscience discovery," *Philos. Trans. R. Soc. B Biol. Sci.* **370**(1668), 20140164 (2015).
2. Z. Fekete, "Recent advances in silicon-based neural microelectrodes and microsystems: a review," *Sens. Actuators, B* **215**, 300–315 (2015).
3. A. S. Herbawi et al., "CMOS-based high-density neural probes with improved scheme for addressing recording and stimulation channels," *Procedia Eng.* **120**, 932–935 (2015).
4. C. M. Lopez et al., "An implantable 455-active-electrode 52-channel CMOS neural probe," *IEEE J. Solid-State Circuits* **49**(1), 248–261 (2014).
5. H. J. Lee et al., "A multichannel neural probe with embedded microfluidic channels for simultaneous in vivo neural recording and drug delivery," *Lab Chip* **15**(6), 1590–1597 (2015).
6. E. Segev et al., "Patterned photostimulation via visible-wavelength photonic probes for deep brain optogenetics," *Neurophotonics* **4**(1), 011002 (2017).
7. R. Scharf et al., "Depth-specific optogenetic control in vivo with a scalable, high-density µLED neural probe," *Sci. Rep.* **6**(January), 28381 (2016).
8. F. Wu et al., "An implantable neural probe with monolithically integrated dielectric waveguide and recording electrodes for optogenetics applications," *J. Neural Eng.* **10**(5), 056012 (2013).
9. G. T. Einevoll et al., "Modelling and analysis of local field potentials for studying the function of cortical circuits," *Nat. Rev. Neurosci.* **14**(11), 770–785 (2013).
10. C. K. Kim, A. Adhikari, and K. Deisseroth, "Integration of optogenetics with complementary methodologies in systems neuroscience," *Nat. Rev. Neurosci.* **18**(4), 222–235 (2017).
11. E. S. Boyden et al., "Millisecond-timescale, genetically targeted optical control of neural activity," *Nat. Neurosci.* **8**(9), 1263–1268 (2005).
12. X. Han, "In vivo application of optogenetics for neural circuit analysis," *ACS Chem. Neurosci.* **3**(8), 577–584 (2012).
13. D. S. Roy et al., "Memory retrieval by activating engram cells in mouse models of early Alzheimer's disease," *Nature* **531**(7595), 508–512 (2016).
14. E. Krook-Magnuson et al., "Cerebellar directed optogenetic intervention inhibits spontaneous hippocampal seizures in a mouse model of temporal lobe epilepsy," *eNeuro* **1**(1), 0005–0014 (2014).
15. M. Scanziani and M. Häusser, "Electrophysiology in the age of light," *Nature* **461**(7266), 930–939 (2009).
16. Y. Son et al., "In vivo optical modulation of neural signals using monolithically integrated two-dimensional neural probe arrays," *Sci. Rep.* **5**(October), 15466 (2015).
17. F. Pisanello et al., "Dynamic illumination of spatially restricted or large brain volumes via a single tapered optical fiber," *Nat. Neurosci.* **20**(8), 1180–1188 (2017).
18. E. Ronzitti et al., "Recent advances in patterned photostimulation for optogenetics," *J. Opt.* **19**(11), 113001 (2017).
19. V. Szabo et al., "Spatially selective holographic photoactivation and functional fluorescence imaging in freely behaving mice with a fiberscope," *Urology* **84**(6), 1157–1169 (2014).
20. E. Claverol-Tinture and Z. Nadasdy, "Intersection of microwire electrodes with proximal CA1 stratum-pyramidale neurons at insertion for multiunit recordings predicted by a 3-D computer model," *IEEE Trans. Biomed. Eng.* **51**(12), 2211–2216 (2004).
21. G. Buzsáki et al., "Tools for probing local circuits: high-density silicon probes combined with optogenetics," *Neuron* **86**(1), 92–105 (2015).
22. F. Wu et al., "Monolithically integrated µLEDs on silicon neural probes for high-resolution optogenetic studies in behaving animals," *Neuron* **88**(6), 1136–1148 (2015).
23. F. Pisanello, L. Sileo, and M. De Vittorio, "Micro- and nanotechnologies for optical neural interfaces," *Front. Neurosci.* **10**(March), 70 (2016).
24. E. Shim et al., "Multisite silicon neural probes with integrated silicon nitride waveguides and gratings for optogenetic applications," *Sci. Rep.* **6**(January), 22693 (2016).
25. D. H. Szarowski et al., "Brain responses to micro-machined silicon devices," *Brain Res.* **983**(1–2), 23–35 (2003).
26. R. A. Rahim et al., "ProTEK PSB coating as an alternative polymeric protection mask for KOH bulk etching of silicon," *Microsyst. Technol.* **19**(6), 905–914 (2013).
27. Z. Liu et al., "Super-selective cryogenic etching for sub-10 nm features," *Nanotechnology* **24**(1), 015305 (2013).
28. R. G. Heideman et al., "TriPleXTM: The low loss passive photonics platform: industrial applications through multi project wafer runs," in *IEEE Photonics Conf.*, pp. 224–225 (2014).
29. C. Rossant et al., "Spike sorting for large, dense electrode arrays," *Nat. Neurosci.* **19**(4), 634–641 (2016).
30. A. Katzir, A. C. Livanos, and A. Yariv, "Chirped-grating output couplers in dielectric waveguides," *Appl. Phys. Lett.* **30**(5), 225–226 (1977).
31. D. J. Edell et al., "Factors influencing the biocompatibility of insertable silicon microshafts in cerebral cortex," *IEEE Trans. Biomed. Eng.* **39**(6), 635–643 (1992).
32. L. P. David and J. Lockwood, *Silicon Photonics II, Components and Integration*, Vol. **94**, pp. 89–91 (2003).
33. L. Fenno, O. Yizhar, and K. Deisseroth, "The development and application of optogenetics," *Annu. Rev. Neurosci.* **34**(1), 389–412 (2011).
34. J. Y. Lin, "A user's guide to channelrhodopsin variants: features, limitations and future developments," *Exp. Physiol.* **96**(1), 19–25 (2011).

Vittorino Lanzio is a nanofabrication researcher and user at the Molecular Foundry, Lawrence Berkeley National Laboratory. He received his master's degree in nanotechnology for information and communication technology (ICT) from Politecnico di Torino and another master's degree in nanosciences from the Universitè Paris-Saclay. His main interests are micro and nanofabrication of optoelectronic devices for neuroscience studies. His main expertise is in device design, nanofabrication, and integrated optoelectronic circuits.

Melanie West is a nanofabrication researcher and user at the Molecular Foundry, Lawrence Berkeley National Laboratory. She received her master's degree in materials engineering from San Josè State University and was a research associate at Crescendo Biosciences, as well as a long-term user at the Molecular Foundry. She has several years of experience in the field of nanofabrication, nanoimprintng, and microfluidics for biological sensing applications.

Alexander Koshelev is a nanophotonics researcher at aBeam Technologies. He received his PhD in optics from Moscow Institute of Physics and Technology and was a lead engineer at Samsung Advanced Institute of Technology, Russia. He has 8 years of experience in the field of nanophotonics. His main expertise is in optical design, nanofabrication and simulation for micro and nanophotonics, as well as for fiber optics.

Gregory Telian received his BS degree in brain and cognitive science from Massachusetts Institute of Technology in 2011. Currently, he is a PhD student in the Adesnik Lab, UC Berkeley. His research focuses on understanding how sensorimotor variables are encoded across connected brain regions during awake behaving contexts.

Paolo Micheletti received his master's degree in nanotechnology for ICTs from the Ecole Polytechnique Federale de Lausanne in 2017. His main research interests are nanotechnologies for biological applications, in particular multifunctional neural probes and electrostimulated drug release from PEDOT nanoparticles.

Raquel Lambert received her master's degree in nanotechnology from the University of Paris-Sud/Paris-Saclay, France, in 2017. Currently, she is a PhD student at Ecole Nationale Supérieure de Chimie de Paris. Her research is centered on the development of molecules combining drugs and imaging probes, to diagnose and treat cancer from *in vitro* to *in vivo* through photodynamic therapy.

Scott Dhuey is a principal scientific engineering associate at the Molecular Foundry, Lawrence Berkeley National Laboratory. His expertise is in nanofabrication techniques, including over 15 years of experience in electron-beam lithography.

Hillel Adesnik is an assistant professor of neurobiology in the Department of Molecular and Cell Biology, UC Berkeley. He has over 16 years of experience in neuroscience research, specifically

in the area of neurophysiology and the function of neural circuits. His laboratory research at the UC Berkeley campus makes extensive use of multielectrode arrays, optogenetics, fluorescence imaging, and pharmacology. He has established a long track record of high-impact publications in his field.

Simone Sassolini is a senior scientific engineer associate at the Molecular Foundry, Lawrence Berkeley National Laboratory. He received his BS degree in aerospace engineering from the Università degli Studi di Perugia. His expertise is in design, simulation, and fabrication of MEMS and x-ray micro- and nano-optics.

Stefano Cabrini is the director of the Nanofabrication Facility, Molecular Foundry, Lawrence Berkeley National Laboratory. He received his PhD in physics (Laurea degree) from the University of Rome "La Sapienza" and was a European postdoc fellow at the Institut d'Optique Théorique et Appliquée, Orsay, France. He has published more than 160 articles on international peer-reviewed journals. He was also a coeditor of the "Nanofabrication Handbook" CRC Press 2012.